Heuristic modelling of laser written mid-infrared $LiNbO_3$ stressed-cladding waveguides

Huu-Dat Nguyen,[1] Airán Ródenas,[1,*] Javier R. Vázquez de Aldana,[2] Javier Martínez,[1] Feng Chen,[3] Magdalena Aguiló,[1] Maria Cinta Pujol[1] and Francesc Díaz[1]

[1]*Física i Cristal·lografía de Materials i Nanomaterials (FiCMA-FiCNA-EMAS), Departament de Química Física i Inorgànica,, Universitat Rovira i Virgili, (URV), 43007, Tarragona, Spain*

[2]*Grupo de Investigación en APLsicaciones del Láser y Fotónica (ALF-USAL), Facultad de Ciencias, Universidad de Salamanca, 37008 Salamanca, Spain*

[3]*School of Physics, State Key Laboratory of Crystal Materials and Key Laboratory of Particle Physics and Particle Irradiation, Ministry of Education, Shandong University, Jinan 250100, China*

[*]*arodenas@gmail.com*

Abstract: Mid-infrared lithium niobate cladding waveguides have great potential in low-loss on-chip non-linear optical instruments such as mid-infrared spectrometers and frequency converters, but their three-dimensional femtosecond-laser fabrication is currently not well understood due to the complex interplay between achievable depressed index values and the stress-optic refractive index changes arising as a function of both laser fabrication parameters, and cladding arrangement. Moreover, both the stress-field anisotropy and the asymmetric shape of low-index tracks yield highly birefringent waveguides not useful for most applications where controlling and manipulating the polarization state of a light beam is crucial. To achieve true high performance devices a fundamental understanding on how these waveguides behave and how they can be ultimately optimized is required. In this work we employ a heuristic modelling approach based on the use of standard optical characterization data along with standard computational numerical methods to obtain a satisfactory approximate solution to the problem of designing realistic laser-written circuit building-blocks, such as straight waveguides, bends and evanescent splitters. We infer basic waveguide design parameters such as the complex index of refraction of laser-written tracks at 3.68 μm mid-infrared wavelengths, as well as the cross-sectional stress-optic index maps, obtaining an overall waveguide simulation that closely matches the measured mid-infrared waveguide properties in terms of anisotropy, mode field distributions and propagation losses. We then explore experimentally feasible waveguide designs in the search of a single-mode low-loss behaviour for both ordinary and extraordinary polarizations. We evaluate the overall losses of s-bend components unveiling the expected radiation bend losses of this type of waveguides, and finally showcase a prototype design of a low-loss evanescent splitter. Developing a realistic waveguide model with which robust waveguide designs can be developed will be key for exploiting the potential of the technology.

OCIS codes: (220.4000) Microstructure fabrication; (160.4330) Nonlinear optical materials; (230.7370) Waveguides; (000.4430) Numerical approximation and analysis.

References and links

1. Y. Ren, G. Brown, A. Ródenas, S. Beecher, F. Chen, and A. K. Kar, "Mid-infrared waveguide lasers in rare-earth-doped YAG," Opt. Lett. **37**(16), 3339–3341 (2012).

#258038 Received 26 Jan 2016; revised 4 Mar 2016; accepted 13 Mar 2016; published 1 Apr 2016

2. R. He, Q. An, Y. Jia, G. R. Castillo-Vega, J. R. Vázquez de Aldana, and F. Chen, "Femtosecond laser micromachining of lithium niobate depressed cladding waveguides," Opt. Mater. Express **3**(9), 1378–1384 (2013).
3. Q. An, Y. Ren, Y. Jia, J. R. V. de Aldana, and F. Chen, "Mid-infrared waveguides in zinc sulfide crystal," Opt. Mater. Express **3**(4), 466–471 (2013).
4. J. R. Macdonald, S. J. Beecher, P. A. Berry, G. Brown, K. L. Schepler, and A. K. Kar, "Efficient mid-infrared Cr:ZnSe channel waveguide laser operating at 2486 nm," Opt. Lett. **38**(13), 2194–2196 (2013).
5. J. Hu and C. R. Menyuk, "Understanding leaky modes: slab waveguide revisited," Adv. Opt. Photonics **1**(1), 58–106 (2009).
6. A. Ródenas, G. Zhou, D. Jaque, and M. Gu, "Direct laser writing of three-dimensional photonic structures in Nd:yttrium aluminum garnet laser ceramics," Appl. Phys. Lett. **93**(15), 151104 (2008).
7. A. Ródenas, G. A. Torchia, G. Lifante, E. Cantelar, J. Lamela, F. Jaque, L. Roso, and D. Jaque, "Refractive index change mechanisms in femtosecond laser written ceramic Nd:YAG waveguides: micro-spectroscopy experiments and beam propagation calculations," Appl. Phys. B **95**(1), 85–96 (2009).
8. A. Rodenas, "Direct femtosecond laser writing of 3D photonic structures in rare-earth doped lithium niobate", PhD Thesis 2009, ISBN 978–84–693–3869–8, *http://hdl.handle.net/10486/4167*
9. A. Ródenas, L. M. Maestro, M. Ramirez, G. A. Torchia, L. Roso, F. Chen, and D. Jaque, "Anisotropic lattice changes in femtosecond laser inscribed Nd^{3+}:MgO:$LiNbO_3$ optical waveguides," J. Appl. Phys. **106**(1), 013110 (2009).
10. B. McMillen and Y. Bellouard, "On the anisotropy of stress-distribution induced in glasses and crystals by non-ablative femtosecond laser exposure," Opt. Express **23**(1), 86–100 (2015).
11. H. Karakuzu, M. Dubov, S. Boscolo, L. A. Melnikov, and Y. A. Mazhirina, "Optimisation of microstructured waveguides in z-cut $LiNbO_3$ crystals," Opt. Mater. Express **4**(3), 541–552 (2014).
12. J. Burghoff, C. Grebing, S. Nolte, and A. Tünnermann, "Efficient frequency doubling in femtosecond laser written waveguides in lithium niobate," Appl. Phys. Lett. **89**(8), 081108 (2006).
13. A. Rodenas, A. Benayas, J. R. Macdonald, J. Zhang, D. Y. Tang, D. Jaque, and A. K. Kar, "Direct laser writing of near-IR step-index buried channel waveguides in rare earth doped YAG," Opt. Lett. **36**(17), 3395–3397 (2011).
14. S. Kroesen, W. Horn, J. Imbrock, and C. Denz, "Electro-optical tunable waveguide embedded multiscan Bragg gratings in lithium niobate by direct femtosecond laser writing," Opt. Express **22**(19), 23339–23348 (2014).
15. A. G. Okhrimchuk, A. V. Shestakov, I. Khrushchev, and J. Mitchell, "Depressed cladding, buried waveguide laser formed in a YAG:Nd^{3+} crystal by femtosecond laser writing," Opt. Lett. **30**(17), 2248–2250 (2005).
16. A. Okhrimchuk, V. Mezentsev, A. Shestakov, and I. Bennion, "Low loss depressed cladding waveguide inscribed in YAG:Nd single crystal by femtosecond laser pulses," Opt. Express **20**(4), 3832–3843 (2012).
17. T. Gorelik, M. Will, S. Nolte, A. Tuennermann, and U. Glatzel, "Transmission electron microscopy studies of femtosecond laser induced modifications in quartz," Appl. Phys., A Mater. Sci. Process. **76**(3), 309–311 (2003).
18. M. Will, J. Burghoff, S. Nolte, A. Tünnermann, F. Wunderlich, and K. Goetz, "Detailed investigations on femtosecond-induced modifcations in crystalline quartz for integrated optical applications," Proc. SPIE **5714**, 261–270 (2005).
19. J. Burghoff, S. Nolte, and A. Tunnermann, "Origins of waveguiding in femtosecond laser structured $LiNbO_3$," Appl. Phys. A **89**(1), 127–132 (2007).
20. Y. S. Kim and R. T. Smith, "Thermal expansion of lithium tantalate and lithium niobate single crystals," J. Appl. Phys. **40**(11), 4637–4641 (1969).
21. A. Ródenas, J. A. Sanz Garcia, D. Jaque, G. A. Torchia, C. Mendez, I. Arias, L. Roso, and F. Agullo-Rueda, "Optical investigations of femtosecond laser induced microstress in neodymium doped lithium niobate crystals," J. Appl. Phys. **100**(3), 033521 (2006).
22. A. S. Andrushchak, B. G. Mytsyk, H. P. Laba, O. V. Yurkevych, I. M. Solskii, A. V. Kityk, and B. Sahraoui, "Complete sets of elastic constants and photoelastic coefficients of pure and MgO-doped lithium niobate crystals at room temperature," J. Appl. Phys. **106**(7), 073510 (2009).
23. D. E. Zelmon, D. L. Small, and D. Jundt, "Infrared corrected Sellmeier coefficients for congruently grown lithium niobate and 5 mol.% magnesium oxide –doped lithium niobate," J. Opt. Soc. Am. B **14**(12), 3319–3322 (1997).
24. Y. Tsuji and M. Koshiba, "Guided-mode and leaky-mode analysis by imaginary distance beam propagation method based on finite element scheme," J. Lightwave Technol. **18**(4), 618–623 (2000).
25. H. Karakuzu, M. Dubov, and S. Boscolo, "Control of the properties of micro-structured waveguides in lithium niobate crystal," Opt. Express **21**(14), 17122–17130 (2013).
26. R. Scarmozzino and R. M. Osgood, "Comparison of finite-difference and Fourier-transform solutions of the parabolic wave equation with emphasis on integrated-optics applications," J. Opt. Soc. Am. A **8**(5), 724–731 (1991).
27. R. Scarmozzino, A. Gopinath, R. Pregla, and S. Helfert, "Numerical techniques for modeling guided-wave photonic devices," IEEE J. Sel. Top. Quantum Electron. **6**(1), 150–162 (2000).
28. G. R. Hadley, "Transparent boundary condition for the beam propagation method," IEEE J. Quantum Electron. **28**(1), 363–370 (1992).
29. S. Gross, N. Jovanovic, A. Sharp, M. Ireland, J. Lawrence, and M. J. Withford, "Low loss mid-infrared ZBLAN waveguides for future astronomical applications," Opt. Express **23**(6), 7946–7956 (2015).

#258038 Received 26 Jan 2016; revised 4 Mar 2016; accepted 13 Mar 2016; published 1 Apr 2016

1. Introduction

The three-dimensional laser writing (3DLW) of mid-infrared (mid-IR) depressed-index cladding waveguides (CLW) in crystals has received considerable attention in recent years, thanks to the easiness with which mid-IR waveguiding can be achieved, and to the potential of the 3DLW technique for fabricating waveguide circuits which are free from the limitations of planar designs and therefore enable the design of circuit architectures hitherto not possible [1–4]. The development of these type of mid-IR waveguides inside the volume of crystalline non-linear optical materials has a wide range of straight applications ranging from novel integrated laser sources to integrated nonlinear frequency conversion chips and electro-optic interferometric spectrometers all exploiting the mid-IR range.

A laser written CLW basically consists on a depressed-index two-dimensional (2D) optical cladding inside which different propagating leaky modes can be sustained depending on the magnitude of the negative refractive index change in the cladding, as well as on the spatial thickness and size of the cladding structure [5]. The exact microstructure of the cladding is made by arranging laser-written tracks, where the permanent refractive index decrease has its origin in the degree of crystal amorphization that results from the strong and spatially localized ionization of the dielectric material and the irreversible lattice damage which is entailed in the energy relaxation processes [6,7]. To achieve an effective sub-micron resolution in the 3DLW process the laser pulse duration is typically kept in the sub-picosecond regime (~0.2 ps) so as to minimize heat affected zones, and the photon energy is usually chosen sub-bandgap ($E_g \approx 3.9$ eV in $LiNbO_3$) so as to attain a laser fluence above the threshold for modification only at the center of the tight focal volume inside the dielectric material, enabling the 3D writing [8].

Although the 3DLW technique is naturally fast and relatively easy to use as compared to clean-room lithography techniques, its transfer to industry as a manufacturing process of anisotropic crystals such as lithium niobate is still far from attainable, due to various bottlenecks regarding the fabrication speed, the reliability of the process as well as the fundamental understanding of the laser interaction processes. One of the challenges which is still to be resolved is the correct understanding of the strong anisotropic stress fields that unavoidably appear alongside any laser-written structures and therefore have to be taken into account when developing laser manufacturing processes of photonic circuits [6–10]. Since the design of mid-IR CLWs involves the microfabrication of structures with sizes in the ~50 μm scale, tens or hundreds of low-index single tracks have to be written to achieve such a large volume. Due to this, the optical properties of fabricated waveguides are typically difficult to predict and very far from what would be expected if no stress-optic index changes are supposed. Since each individual track is a source of anisotropic stress-fields, the overall stress field built up in the full cladding structure will depend on the exact 2D track arrangement and therefore the final optical properties of the waveguides cannot be reliably predicted, unless a comprehensive stress-optic waveguide model is built in advance. This difficulty implies that up until now all experimental reports on CLWs have been performed following a trial and error methodology where the exact processes involved in the fabrication of the guiding structure are not well understood, and as a result the development of a comprehensive model on which to build a reliable manufacturing process has not been achieved. In this sense, a systematic study on CLWs with the aim of developing a realistic model on how both the laser-written depressed index map and the stress-optic index maps form and combine as a function of the basic laser parameters has hitherto not been performed. Furthermore, such a knowledge is deeply required for the development of specifically mid-IR waveguides, since at this larger wavelength range the confinement losses of CLWs are larger than at the near-IR or visible ranges [11], and therefore the cladding microstructure design has to be necessarily optimized in a comprehensive way so as to obtain low propagation losses below the 0.5 dB/cm level typically required for optical circuits of cm's size.

#258038 Received 26 Jan 2016; revised 4 Mar 2016; accepted 13 Mar 2016; published 1 Apr 2016

Up until the first report on the use of a laser-written crystalline CLW for guiding in the mid-IR range [1], the longest operating wavelength in a crystalline 3DLW waveguide was limited to around ~1.5 μm, and was obtained by using the standard double-track stress-optic waveguiding approach (see Fig. 1 below), first reported by Burghoff et al. in $LiNbO_3$ crystals for ~1 μm wavelength light [12]. The stress-optic double-track approach was however proven to be insufficient for confining 1.9 μm near-IR light [13], and recently Kroesen et al. experimentally showed how at 1.55 μm the CLW design gives comparatively much better waveguiding performance (in terms of propagation losses and waveguide anisotropy) than the two-track approach [14]. Although the seminal introduction of the CLW approach was performed by Okhimchuck et al. a decade ago with the intention of developing compact and efficient Nd:YAG waveguide lasers at 1.06 μm [15,16], only recently the approach has been used for demonstrating efficient crystalline channel waveguide lasers at longer wavelengths (waveguide lasing in Tm:YAG crystals at 1.9 μm as well as Cr:ZnSe crystals at 2.5 μm [1,4]). In this sense, the CLW is indeed advantageous for laser applications due to the fact that both the mode spatial distribution and size can be easily tailored for achieving optimal input coupling and efficient lasing and also because the core is made of pristine material. However, besides laser applications the fabrication of low-loss mid-IR $LiNbO_3$ CLWs is also highly desirable for developing high-performance and monolithic mid-IR non-linear chips.

1.1. Difficulties in achieving laser-written crystalline low-loss mid-IR cladding waveguides

The development of low propagation loss (~0.5 dB/cm) laser-written LiNbO3 CLWs for the mid-IR range is strongly limited by the reported difficulty of achieving propagation losses below 3 dB/cm at wavelengths larger than ~3 μm. In the first report on $LiNbO_3$ mid-IR CLWs only insertion losses (IL) were reported, with a value of ~5 dB for a 1 cm long single mode CLW at 4 μm wavelength [2]. Recently, An et al. reported single mode CLWs on ZnS crystals with PLs ~4 dB/cm at 4 μm [3]. Beyond these experimental reports, Karakuzu et al. recently performed a systematic confinement-loss numerical calculation on $LiNbO_3$ crystals, concluding that only PLs ≥1 dB/cm are theoretically possible at 3.5 μm wavelength [11]. This theoretical work however did not take into account the characteristic stress-fields which affect guiding structures fabricated by 3DLW [7–11], and was also built on a different CLW design composed of seven ring layers with circular rod shapes. At the light of these results, achieving low-loss (PLs<0.5 dB/cm) mid-IR CLWs in $LiNbO_3$ is undoubtedly a challenge which needs to be tackled and whose solution requires a deeper understanding of the real refractive index changes that occur at the mid-IR range. Moreover, there has been no study to our knowledge on the expected bend radiation losses of this type of crystalline CLWs in the mid-IR range, which is also a fundamental issue which needs to be optimized for achieving mid-IR on-chip circuits. Achieving a general understanding of how to model these type of waveguides would allow to perform realistic numerical calculations towards their optimization.

In this work we report on a heuristic approach for the modelling of mid-IR $LiNbO_3$ CLWs, i.e. a method for achieving satisfactory solutions to the complex problem of predicting the optical behavior (modal properties, birefringence, propagation losses and bend radiation losses) of mid-IR CLWs. We use experimental data such as the waveguide mode near field intensity distributions and the PLs of fabricated waveguides, together with stress field values from previous studies, and compare this measured data with that obtained from a first waveguide model using standard computational tools as the finite element method (FEM) and the finite difference beam propagation method (FD-BPM). Iterations of the waveguide parameters are then run until the model results match the experimentally measured data. Once the waveguide parameters match the experimental data obtained with our laser system, we then subsequently explore different cladding designs in the search for a low-loss behavior for both transverse magnetic (TM) and electric (TE) polarized modes. For each cladding design we also evaluate the expected overall losses of s-bend components, and finally we showcase a 3.68 μm wavelength 50:50 low-loss evanescent splitter based on low-loss CLWs.

#258038 Received 26 Jan 2016; revised 4 Mar 2016; accepted 13 Mar 2016; published 1 Apr 2016

2. Numerical simulation models

2.1 Finite Element Method (FEM) simulation of anisotropically stressed cladding waveguides

2.1.1 Stress field simulation

The numerical analysis of the waveguides was performed with commercial COMSOL Multiphysics® software. The tight focusing of femtosecond laser pulses inside $LiNbO_3$ is well known to induce a micrometric volume change, which resembles the laser focus ellipsoid, and consists on lattice damaged crystal where slight amorphization occurs and is surrounded by a characteristic anisotropic stress field [9,17–19]. The local volume changes surrounding a longitudinal and straight laser-written track can therefore be simulated with a 2D thermal expansion model, supposing that the amorphized volume expands and elastically distorts the surrounding unmodified crystal, simplifying the problem to a 2D cross-sectional calculation. This approach was first validated for two-track waveguide designs in the visible and near-IR range by Gorelik et al. and Will et al. in quartz crystals [17,18], and subsequently by Burghoff et al. in $LiNbO_3$ crystals [19]. Due to the fact that real track shapes strongly vary depending on the type of laser writing system used as well as crystal composition and crystallographic orientation [8,19], these simulations need to be performed with a well characterized sample and under well specified 3D laser fabrication system parameters. In our case, the laser-written tracks were simulated to have elliptical shape with length of 20 μm along the incident direction of laser beam (z-axis, vertical) and width of 1 μm along the perpendicular direction (y-axis, horizontal). These dimensional values were obtained from arrays of fabricated tracks and waveguides and characterized with back-scatter SEM imaging (not shown here for the sake of brevity). The experimental set up is described in Section 3. The simulation is governed by the Hooke's law [Eq. (1)] which reflects the relation between strain (ε), stress (σ), tensors and temperature difference in linear thermal expansion model.

$$\sigma_{ij} = \sigma_0 + C_{ijkl} : \left(\varepsilon_{kl} - \varepsilon_0 - \alpha_{kl}\theta\right). \tag{1}$$

where C_{ijkl} is the fourth order elasticity tensor, ":" stands for the double-dot tensor product, σ_0 and ε_0 are initial stress and strain, θ is the temperature change parameter controlling the expansion $\theta = T - T_0$, and α_{kl} is the second order linear thermal expansion tensor. The elasticity tensor can be completely represented by a known symmetric 6x6 matrix [20], and the thermal expansion coefficients were taken from [21]. For the case of the strain tensor, it is written in terms of the point displacement gradient ∇u :

$$\varepsilon = \frac{1}{2}\left(\nabla u + \nabla u^T\right); \varepsilon_{mn} = \frac{1}{2}\left(\frac{\partial u_m}{\partial u_n} + \frac{\partial u_n}{\partial u_m}\right). \tag{2}$$

A fixed constraint is set at an outer boundary of circular shape and domain size of 0.6 mm diameter, and a displacement constraint is assigned to the laser-written track domains where the expansion starts. The temperature difference θ is used as a primary control parameter that can be set to match experimental data, for example simulating a pair of written tracks (see Fig. 1) where the stress field has been experimentally studied [8,19]. In this first study, we have used available micro-stress data from previous laser-written waveguides in $LiNbO_3$ crystals with the same fabrication parameters to those of the present work. These works revealed that the range of induced stress field magnitudes between a pair of tracks that are separated by several micrometers (~10-50 μm) and that are fabricated using chirped pulse amplified laser systems delivering near-IR (~800 nm) sub-picosecond (~200 fs) low-repetition rate (~1 KHz) pulsed laser trains, and written with standard focusing lenses (~0.2-0.6 NA), is of the order of 10-500 MPa depending on the selected laser pulse energy (typically ~0.1-0.8 μJ) [8,19,21]. We nonetheless notice that a more detailed stress-field distribution study is still lacking for the case of laser-written $LiNbO_3$ crystals, which could be done by using novel rapid stress analysis methods such as those reported by McMillen et al [10].

#258038 Received 26 Jan 2016; revised 4 Mar 2016; accepted 13 Mar 2016; published 1 Apr 2016

2.1.2 Mode analysis simulation

The obtained 2D stress distribution is assumed as the only responsible field for refractive index (RI) changes surrounding the laser inscribed low-index tracks. The relationship between stress-induced RI changes and stress tensor is governed by the piezo-optic effect:

$$\Delta\left(\frac{1}{n^2}\right)_{ij} = \sum_{k,l} \pi_{ijkl}\sigma_{kl}. \tag{3}$$

where the piezo-optic tensor π_{ijkl} of the material is taken from [22].

Inside the tracks, a decrease of the real part of the $LiNbO_3$ RI of around 0.01-0.001 is known to occur as a result a $LiNbO_3$ crystalline lattice damage and amorphization [8,19]. The precise knowledge of these values is however still subject of research, due to the fact that the exact physical processes that the $LiNbO_3$ lattice undergoes when exposed to different types of tightly focused fs laser pulsed beams are not known, and there is a clear lack of available techniques capable of directly measuring the refractive index values of high index materials with a sub-μm spatial resolution, as required for this type laser written structures. Moreover, it is also of paramount importance to differentiate among the RI change values measured at the visible, near-IR, or mid-IR wavelength ranges, since these ranges involve fundamentally different resonance effects, such as the bandgap absorption at the UV-vis and impurities, lattice defects absorptions, and multiphonon absorptions in the mid-IR, so that RI values measured using visible light instruments may not be valid for characterizing mid-IR waveguides. Nevertheless, due to the lack of direct RI measurements of laser-written $LiNbO_3$ structures in the mid-IR range, in this work we start the model using already reported RI values at visible light experiments as input parameters [19], and later refine these values in iterative steps to match our experimental mid-IR waveguide characterization results. It is pertinent to recall here the fundamental difference between guided modes in RI increased core waveguides (such as in the case of double-track stress-optic waveguides) where waveguiding of a confined mode is achieved in the high RI $LiNbO_3$ volume, and the leaky modes of depressed index CLWs, where light propagation takes place within a core volume which has the same RI as the rest of the crystalline material and only a continuum of radiation modes exists inside the low RI cladding. In this sense, while confined modes rely on the magnitude of the positive RI increase at the core, the leaky modes of CLWs are very sensitive to the magnitude of the negative RI change inside the tracks conforming the cladding [5]. It is in this regard that choosing CLWs as object for studying the unknown mid-IR RI change values of laser micro-processed $LiNbO_3$ can be a powerful indirect method.

The electromagnetic-wave frequency-domain model was applied for the analysis of mode guiding. All simulations in this work are computed for a free space wavelength of 3.68 μm and the $LiNbO_3$ refractive indices of n_z = 2.0700 and n_y = 2.1309 for extraordinary and ordinary polarized modes, respectively [23]. In order to truncate the computational domain and minimize light reflections from the boundary, isotropic and circular perfectly matched layers (PML) where applied surrounding the cladding waveguide structure. The PML light absorber is defined as a function of refractive index n_{PML} [24,25]:

$$n_{PML}(r) = n_{o,e} - ik_{\max}\left(\frac{r - r_{in}}{L}\right)^2, r_{in} < r \le r_{in} + L. \tag{4}$$

where r is the radial coordinate, r_{in} and L are the inner radius and thickness of the PML, and k_{max} is the maximum absorption value. All these parameters have been carefully chosen so as to give reliable waveguide modes [5]: k_{max} = 0.002 has been chosen as giving the most effective absorption for the structure, and r_{in} = 150 μm and L = 150 μm are chosen to effectively reduce the computational domain while not affecting the computed modes. Since the laser-written tracks were simulated to have a considerably elliptical shape with width of

#258038 Received 26 Jan 2016; revised 4 Mar 2016; accepted 13 Mar 2016; published 1 Apr 2016

~1 μm along the perpendicular direction (y-axis, horizontal) and ~20 μm along the incident (writing) direction of the laser beam (z-axis, vertical), the finite elements mesh of elliptical tracks was defined with a free triangular mesh of size around 40 nm in the horizontal and 450 nm for the vertical. Inside the cladding area a free triangular mesh of size around 1 μm in both horizontal and vertical directions was used. The rest of domains were defined with free triangular meshes of minimum size 50 nm and maximum size 10 μm. The initial refractive index changes (Δn) assumed at the tracks for the mid-IR range, were of $\Delta n = -5 \times 10^{-3}$ for both polarizations. TM and TE modes were studied separately, and iteratively computed varying the Δn values, to match experimental results by varying the Δn values of the laser-written tracks. In the first mode analysis we typically searched for as many modes as possible (~500 modes). From this first simulation it was then possible to refine the effective index and use this value for further simulations in which only 20 modes were looked for and the time consumption for simulation could be reduced.

2.2 Light propagation simulation

Light propagation was simulated by BeamPROP software which is a part of the RSoft Photonic Component Design Suite®. The computational simulation is based on FD-BPM and a transparent boundary condition was applied, following previous works [26–28]. For a straight waveguide, a simple segment was created with total length of 22 mm. The segment was assigned to the complex RI profile of the designed cladding structure previously generated by COMSOL model and which was processed in Matlab to create a readable BeamPROP matrix file. This methodology allowed to apply any specific designated complex index profile which cannot be done by using simple built-in drawing tools. For large radii bend waveguides (R ≥100 mm) the same procedure was applied and a circular s-bend was added between the input and output straight sections. Scaling and grid sizes were thoroughly considered to assure that correct computations were obtained. Mode solving was performed by launching a gaussian field in the waveguide input and using correlation method. The use of a correlation method is suitable for finding lossy or leaky modes. For the simulation of light propagation, the obtained fundamental mode (FM) was launched in the waveguide input, while the output power was monitored along the waveguide pathway, using a square monitor of the size of the corresponding waveguide core. All beam propagation Figs. in this work show a 2D intensity distribution across the waveguides, i.e. the near-field intensity distribution inside the CLWs, and the integrated power across the monitor surface, which represents the actual power flux at each point along the waveguide path length. This allowed us to compare the propagation losses (PLs) of different cladding designs. Bend losses (BLs) were also estimated by subtracting the PLs of straight waveguides to the total loss obtained in an s-bend waveguide of equal length. By knowing the total extra radiation loss due to bends we then normalize this value to the total arc length of the s-bend in mm, obtaining a BLs value in dB/mm. Besides this method, we also estimate the straight waveguide mode PLs by assuming an exponential decay with propagation length with the effective medium attenuation coefficient $\alpha = 4\pi \cdot Im(n_{\text{eff}})/\lambda$, so that:

$$PLs(dB/cm) = \frac{40\pi}{\ln 10.\lambda(\mu m)} Im(n_{eff}) \times 10^4. \quad (5)$$

and which gave equivalent numerical results.

3. Experimental and technical details

3.1 Laser fabrication of the cladding waveguide structures

Cladding structures were formed by transversally writing tracks to form a depressed-index circular tubular array that can sustain leaky modes. Due to the high anisotropy of the track cross section, the dimension of the resulting cladding is much larger in the vertical than the

#258038 Received 26 Jan 2016; revised 4 Mar 2016; accepted 13 Mar 2016; published 1 Apr 2016

horizontal cross section, therefore extra lines of tracks were added to the lateral sides of the circular shape structure so that this asymmetry can be minimized within this simple laser writing setup (see Fig. 2). Single tracks were first written so as to obtain the track sizes as a function of laser power and focusing depth for a fixed scanning speed of 0.7 mm/s. Subsequently, CLWs with diameter core sizes of 40 μm, 70 μm and 110 μm were designed in COMSOL and the tracks coordinates where then used in the laser inscription process. In this paper we only report the smallest fabricated waveguides (diameter core of 40 μm, named as 40-CLW), since the others were multimode and therefore out of the interest of the present work.

A Z-cut MgO:$LiNbO_3$ sample was cut with dimensions of 20(x) × 10(y) × 1(z) mm^3 and optically polished. 3DLW was performed along the z-axis of the sample. A Ti:Sapphire regenerative amplifier laser system (Spitfire and Tsunami systems, Spectra-Physics) was used. The system produces linearly-polarized pulses of about ~120 fs duration, with a repetition rate of 1 kHz at a central wavelength around 795 nm. A calibrated neutral density filter, a half-wave plate and a linear polarizer were used to precisely control the value of the pulse energy. The sample was mounted on a high-resolution three-axis motorized stage. The laser beam was focused through the xy plane of the sample at a minimum depth of 300 μm using a microscope objective (20x, N.A = 0.4). Waveguides were written along the 20 mm x-axis long dimension of the crystal. Track separation in the y-direction was fixed to 2 μm. The writing speed was of 0.7 mm/s and the pulse energy was set to 0.6 μJ. Laser polarization was kept perpendicular to the scanning direction. After fabrication the end facets of the sample were polished.

3.2. Optical waveguide characterization

The mid-IR guiding properties of CLWs were characterized using a linearly polarized ICL diode-laser (Nanoplus) emitting at the wavelength of 3.683 μm. The sample was mounted on a Thorlabs stage with 5-axis microcontrollers. Input and output laser coupling was performed using aspheric lenses (C021TME-E, NA = 0.18) from Thorlabs. Imaging was performed on a FLIR SC7000 mid-IR camera. In order to optimize the CLW mode excitation and minimize the excitation of cladding modes, a pinhole was used before the input lens to finely adjust the beam diameter. The input coupling efficiency was calculated by the overlap integral method for ten different pinhole diameters, using the measured laser input focal spots and the waveguide output mode. The insertion losses were measured for all pinhole diameters to verify the optimum coupling, and a minimum of 4.1 dB was achieved when the input spot field diameter closely matched the 40-CLW mode field diameter (MFD). PLs were calculated by subtracting the coupling losses and the Fresnel losses to the insertion losses. To obtain calibrated MFDs a calibration target was used (R1DS1P - Positive 1951 USAF Test Target, Ø1").

4. Results

4.1 Simulated total stress field of two adjacent parallel tracks

The simulation for two adjacent parallel tracks was performed as starting step because these type of waveguides are very well known and studied, and the main features of the total stress fields, such as anisotropy and the typical experimental levels of stress field magnitudes can be obtained from literature [8,19,21]. Running this first simple array allows to obtain a starting value for the main parameter of the CLWs simulation, which is the temperature difference (θ), which controls the stress level, and can be set to obtain a value that matches previously reported values. The simulation results of the obtained stress field built up around 2 elliptical parallel adjacent tracks with a separation of 10 μm are shown in Fig. 1.

#258038 Received 26 Jan 2016; revised 4 Mar 2016; accepted 13 Mar 2016; published 1 Apr 2016

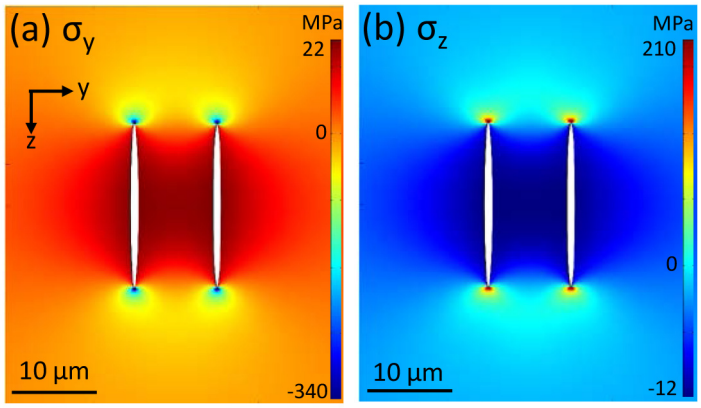

Fig. 1. Simulated stress field of the 2-track structure. (a) for the σ_y component (b) for the σ_z component.

It can be seen that for the σ_y stress component, compressive stress is distributed along the lateral side of the tracks, while tensile stress takes place at the apexes. For the σ_z stress component, the stress is tensile between the tracks and compressive at the tracks apexes. The temperature difference (θ) parameter was set to 100 K, which produces a compressive stress value (σ_y) of around 20 MPa between tracks, in a good agreement with previous work using the same experimental setup [8].

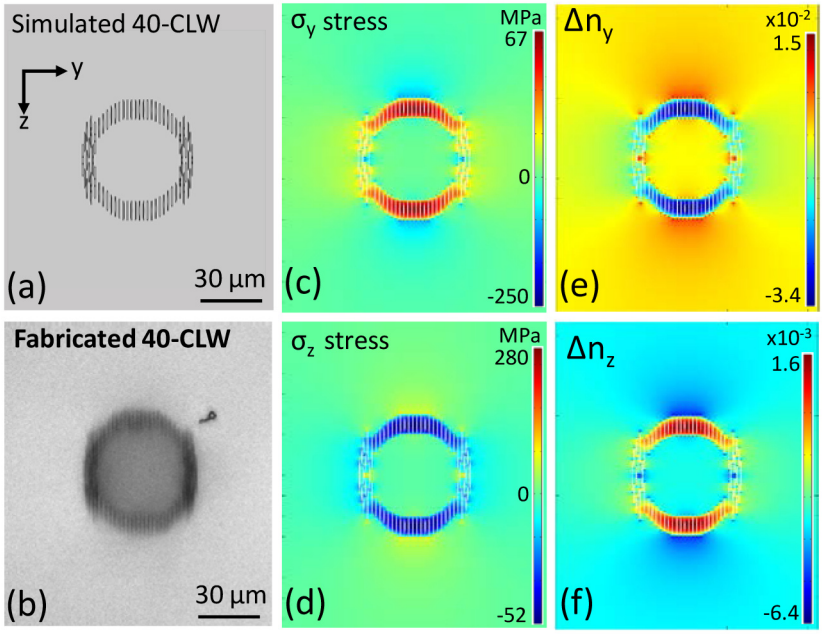

Fig. 2. Profiles of 40 µm diameter core cladding waveguides: (a) geometry, (b) fabricated result, (c)(d) stress fields σ_y and σ_z, (e)(f) stress-optic refractive index change distributions n_y and n_z.

4.2 Stress field in the cladding structures

The 40-CLW cladding geometry is displayed in Fig. 2(a), being very well matched with the real cladding fabricated by 3DLW shown in Fig. 2(b). The cladding ring is formed by 79 elliptical tracks (with horizontal track separations of 2 µm) including extra lines of tracks at

#258038 Received 26 Jan 2016; revised 4 Mar 2016; accepted 13 Mar 2016; published 1 Apr 2016

the sides which aim to "strengthen" the cladding wall. As it can be seen in Fig. 2(c) and (d), a biaxial tensile/compressive $\sigma_{y/z}$ stress field develops at the top and bottom sides of the cladding. This stress field will produce a strongly anisotropic waveguide behaviour. The maximum compressive and tensile stress is of about 67 MPa and 280 MPa, respectively. RI change profiles resembling the stress fields are shown in Fig. 2(e) and (f). It is also observed that changes of RI in the inside of the cladding ring are smaller than those outside. This is explained by the fact that the stress field originating from the inside apexes is partly cancelled by the opposite stress from the neighbour tracks due to the circular geometry. From this first analysis it is clear that the cladding confinement will be more efficient for TE-polarized modes, than for TM. This effect does not depend on the $LiNbO_3$ crystallographic axial alignment; it is an anisotropic effect arising solely by the highly asymmetric shape of the tracks. By placing the tracks closer together this effect can be mitigated, however at the cost of duplicating the fabrication time, and also increasing the risk of sample cracking. To avoid these two issues and maintain flexible fabrication parameters which do not entail cracking, in this work we have fixed the distance between tracks to 2 μm for all the studied cladding designs.

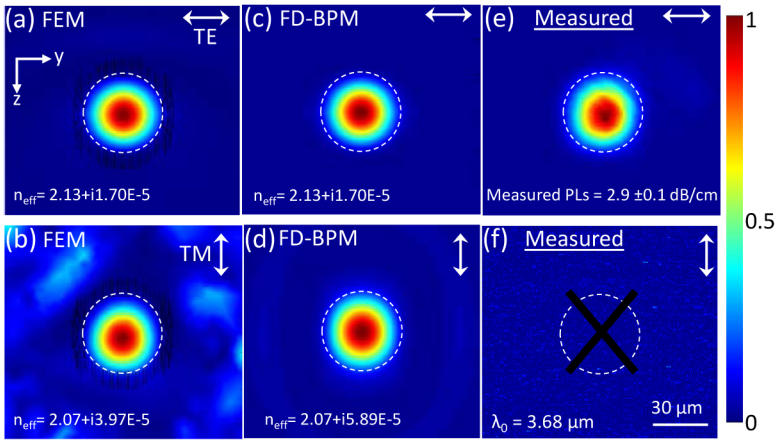

Fig. 3. Fundamental mode near field intensity distribution of the 40 μm diameter core CLW as obtained by FEM (a and b), FD-BPM (c and d), and experiments (e, and f).

4.3. Optical mode analysis and propagation losses in the cladding structures

A first mode analysis was performed both with FEM and FD-BPM software, using the initial parameters (see Section §2 for details), and compared with the real optical measurement of the fabricated 40-CLW. Fig. 3 shows a summary of results comparing the simulated TE and TM fundamental modes by the FEM method [Fig. 3(a) and (b)], FD-BPM method [Fig. 3(c) and (d)], and experimental results [Fig. 3(e) and (f)]. The effective index of the modes was obtained by both FEM and FD-BPM giving a TE mode with an effective refractive index of $2.13 + i1.7 \times 10^{-5}$. The imaginary part of the effective refractive index gives an estimated PLs of 2.5 dB/cm, which is slightly lower than the measured value (2.9 ± 0.1 dB/cm). In the case of vertically polarized light no TM mode was observed experimentally, while the PLs of the TM mode is calculated to be around 8.7 dB/cm. The reason why the 40-CLW does not guide TM light could be either that the losses are too high for this polarization and/or that the index change inside the tracks for vertically polarized (n_e) light is significantly lower than that for horizontally polarized light, so that the minimum index contrast for sustaining a leaky mode at 3680 nm wavelength is not attained. The 40-CLW seems to guide well TE polarized light. The measured propagation losses of 2.9 dB/cm is a value comparable with previous reported values [2,3,11], and in line with the observation described in Section §1.1 that losses below 1

#258038 Received 26 Jan 2016; revised 4 Mar 2016; accepted 13 Mar 2016; published 1 Apr 2016

dB/cm at mid-IR wavelengths appear to be hardly achievable so far, by the 3DLW technique in crystals.

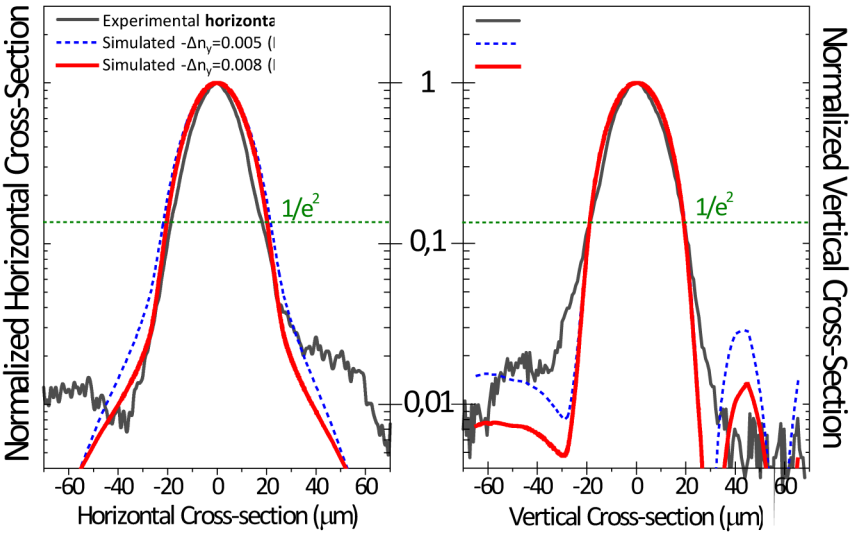

Fig. 4. Comparison of near field TE mode cross sections of simulations and experiment. Horizontal cross sections are shown on the left and vertical cross sections are shown on the right. The best matching between simulated and measured cross sections was obtained for an index change inside tracks of $\Delta n = -0.008$.

4.4. Refinement of the model: the complex index of refraction of laser modified $LiNbO_3$

Since the experimental characterisation of the 40-CLW showed no TM mode, only TE modes were used for further improving the model parameters. In the following we compare the cross sections of the experimental TE mode near field with the simulated ones, with the aim of obtaining the refractive index of laser modified depressed index tracks which give a best fit of the model. Fig. 4 shows the horizontal cross sections on the left, and vertical cross sections on the right. As it can be seen, the initial assumption that the Δn inside the tracks $\Delta n = -0.005$ gives a good matching between the simulated and the measured vertical MFD of the TE mid-IR mode. However, in the following we evaluate its optimization using the model and the experimental measurements. A set of different TE modes was computed for varying Δn_y values inside tracks from -0.001 to -0.01, so as to obtain the best overall fit to the measured near field mode. The best MFD matching was obtained for a Δn inside tracks of -0.008 (red line in Fig. 4). In this case, the vertical MFD is of 38.2 µm for both simulation and experiment, and of 40.6 µm (simulation) and 37.0 µm (experiment) along the horizontal direction. From this experiment we therefore conclude that the ordinary Δn_y of laser modified $LiNbO_3$ which forms the cladding has a reduced index of -0.008, at 3.68 µm wavelength. For the case of extraordinary light, since we did not obtain experimental data we will use the same value as a first approximation. In this regard, it is worth noticing that small variations in the Δn of ± 0.002 at tracks do not significantly affect the MFDs, so that this parameter is not highly critical for designing this type of CLWs.

#258038 Received 26 Jan 2016; revised 4 Mar 2016; accepted 13 Mar 2016; published 1 Apr 2016

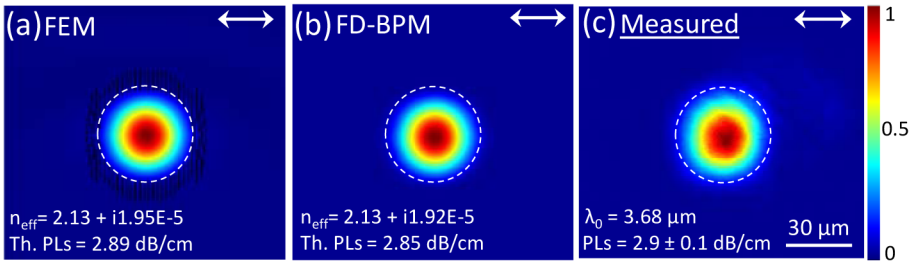

Fig. 5. Simulated (a and b) and measured (c) TE modes of the 40-CLW. (a) FEM, (b) FD-BPM and (c) experiment. Using complex RI change inside the cladding tracks: $\Delta n_y = -0.008 + i0.0007$. Scale bar in (c) is 30 µm and it is the same for the three Figs.

Since the simulation was performed in a purely refractive structure and the obtained waveguide losses are purely confinement losses, adding an imaginary component to the index of refraction (extinction coefficient associated to the absorption and scattering at the tracks volume) of damaged $LiNbO_3$ at cladding tracks will allow to better predict the real losses from the model. A set of ten different complex refraction indexes inside the tracks was run, with varying imaginary part from 10^{-4} to 10^{-5}. The final theoretical propagation losses of the TE modes were obtained both from formula (5), and from BeamPROP calculations. The optimized RI change value at the tracks was found to be $\Delta n_y = -0.008 + i7 \times 10^{-4}$, which gives a TE mode effective refractive index of $2.13 + 1.95 \times i10^{-5}$. This TE mode effective index gives a propagation loss of 2.89 dB/cm, in excellent agreement with the measured value of 2.9 ± 0.1 dB/cm. The final results of the simulated TE and the measured mode are shown in Fig. 5.

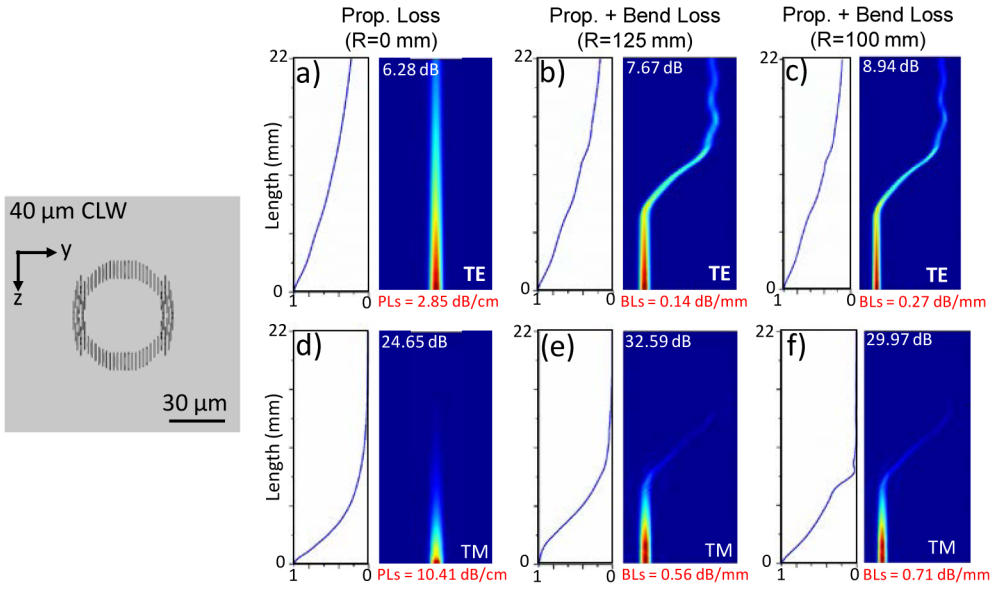

Fig. 6. Straight waveguide propagation losses (a and d), s-bend with R = 125 mm (b and e), and s-bend with R = 100 mm (c and f). Propagation losses (PLs, dB/cm straight length) and bend losses (BLs, dB/mm arc length) are evaluated for TE and TM modes.

#258038 Received 26 Jan 2016; revised 4 Mar 2016; accepted 13 Mar 2016; published 1 Apr 2016

4.5 Simulation of s-bend losses of mid-IR $LiNbO_3$ cladding waveguides

4.5.1 Simulation of s-bend losses of 40 µm diameter core cladding (40CLW)

The 40 µm core diameter waveguide 40CLW with a 22 mm length was first simulated. All results are shown in Fig. 6. The waveguide index profiles are taken from COMSOL results along with the $\Delta n = -0.008 + 0.0007i$ at laser written tracks. The bend waveguides have 0.2 mm offsets to the sides, and radii of 125 and 100 mm are evaluated. For TE polarization, PLs are of 2.85 dB/cm close to the measured value (2.9 dB/cm). We obtain a TE mode BLs of 0.14 and 0.27 dB/mm for 125 and 100 mm radii, respectively. For the TM mode, we obtain a PLs of 10.41 dB/cm, and BLs of 0.56 and 0.71 dB/mm for 125 and 100 mm, respectively.

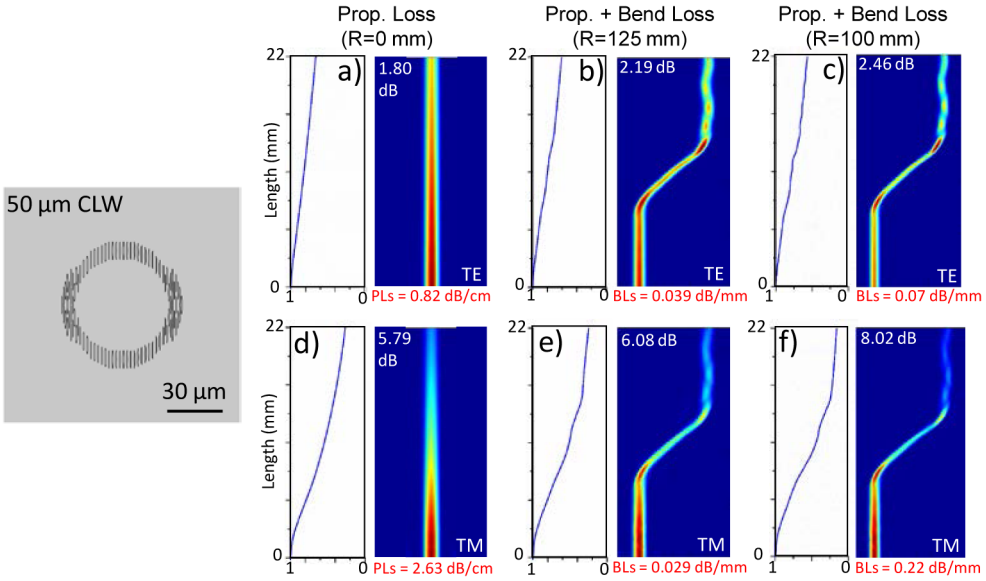

Fig. 7. Straight waveguide PLs (a and d), s-bend with R = 125 mm (b and e), and with R = 100 mm (c and f).

4.5.2 Simulation of 50 µm diameter core cladding (50-CLW)

A simulation of 50 µm diameter core diameter cladding waveguide was also performed. Fig. 7 shows all results. Only one higher mode was observed with a high imaginary effective index of ~3×10^{-4} and which therefore we expect to be not relevant for the present analysis. The PLs of the fundamental mode are of 0.82 dB/cm and 2.63 dB/cm for TE and TM modes, respectively. The bend losses are also improved in both cases: TE mode BLs of 0.039 and 0.07 dB/mm for 125 and 100 mm radii, respectively; and TM mode BLs of 0.029 and 0.22 dB/mm for 125 and 100 mm, respectively. The threshold of 0.5 dB/cm PLs that we established for considering acceptable device losses is however not achieved. Furthermore, the waveguide is still highly anisotropic with high PLs for TM light. A much wider cladding design is therefore required.

4.5.3 Simulation of a 50 µm diameter core double ring cladding (50-CLW2R)

The attenuation of leaky modes is known to be exponential with a rate rapidly decreasing as the thickness of the depressed index cladding increases [5]. Therefore, it is straightforward to fabricate lower PLs CLWs by just increasing the number of tracks conforming the cladding layer. This procedure is however at the cost of greatly increasing the fabrication time. Therefore, our model proves to be useful in this regard allowing one to first test a low-loss CLW design with a minimized number of tracks. Recently, Gross et al. reported the lowest

#258038 Received 26 Jan 2016; revised 4 Mar 2016; accepted 13 Mar 2016; published 1 Apr 2016

loss so far mid-IR CLWs fabricated by means of 3DLW (to the best of our knowledge), using ZBLAN glass [29]. Low PLs of 0.29 dB/cm were experimentally measured for a 47 µm diameter core and 59 µm thickness circular depressed CLW at the wavelength of 4 µm. To further decrease the PLs of $LiNbO_3$ CLWs we therefore increase the cladding thickness wall, but limited it to 14 µm so as maintain a reasonably low chip fabrication time. The thickness enlargement was obtained by incorporating a second ring of tracks to the cladding design, and obtaining a circular cladding similar to the one fabricated in ZBLAN glass by Gross et al. [29]. Fig. 8 shows all results of this 50-CLW2R design. The simulation of this 50-CLW2R cladding yields a TE mode PLs of 0.41 dB/cm, and a TM mode PLs of 0.88 dB/cm, therefore achieving low enough PLs for device developments. Regarding the BLs, for 125 mm and 100 mm radii, the TE mode BLs are of 0.03 and 0.05 dB/mm, and the TM mode BLs are of 0.02 and 0.04 dB/mm, respectively.

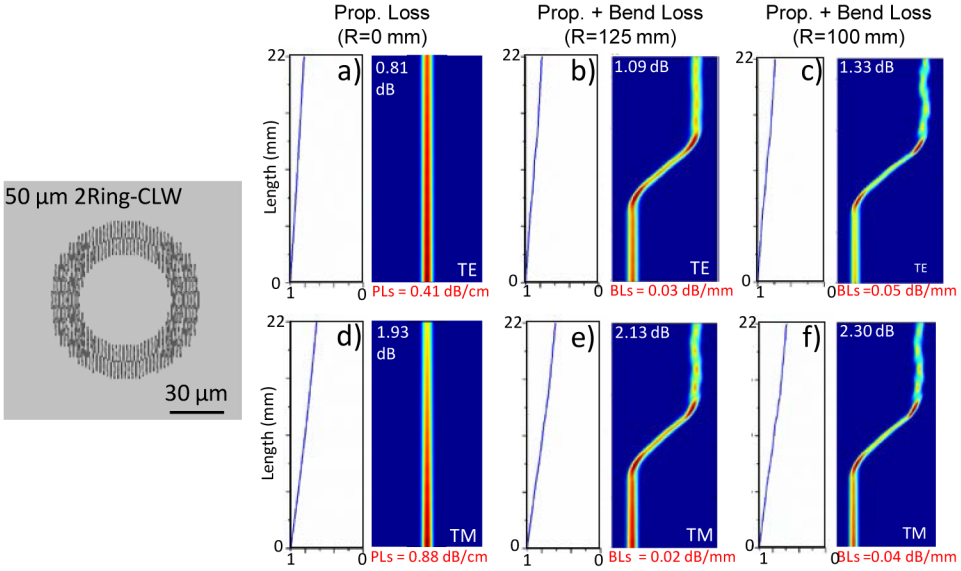

Fig. 8. Simulation of light propagation in the 50 µm diameter core straight waveguide and s-bend double ring CLW. Straight waveguide propagation losses (a and d), s-bend with r = 125 mm (b and e), and s-bend with r = 100 mm (c and f). Propagation losses (PLs, dB/cm straight length) and bend losses (BLs, dB/mm arc length) are evaluated for TE and TM modes.

4.6 Simulation of a 50:50 directional splitter

Finally, we have studied the evanescent coupling behavior of double ring CLWs at 3.683 µm wavelength, and simulated a 50:50 directional splitter for TE modes. In order to ensure single mode profile along the evanescent coupling section, waveguides are designed with core diameter of 36 µm and double cladding structure for this splitting section. The separation of the two waveguides in the coupling region is maintained to 38 µm from center to center which leaves only 1 low index track between them [see Fig. 9(a)]. The 50:50 directional splitting is achieved by introducing two s-bends to the two waveguide branches once a half coupling length has been reached. The 290 µm separation of the waveguides is achieved with bend radius of 71.4 mm after 6 mm length of propagation [see Fig. 9(a)]. Fig. 9(b) and (c) show the behavior for the TE polarized mode: the directional coupling region has a half coupling length (50% power transmission) of 3.285 mm, and the total element including the straight input and output regions has a total excess loss [= $10*\log(P_{in}/(P_{out1} + P_{out2})$] of 1.9 dB for the chosen length of 9.4 mm. This result demonstrates that it is possible to design beam splitting waveguide circuits capable of operating at the mid-IR range, for the first time to our knowledge, in $LiNbO_3$ crystals.

#258038 Received 26 Jan 2016; revised 4 Mar 2016; accepted 13 Mar 2016; published 1 Apr 2016

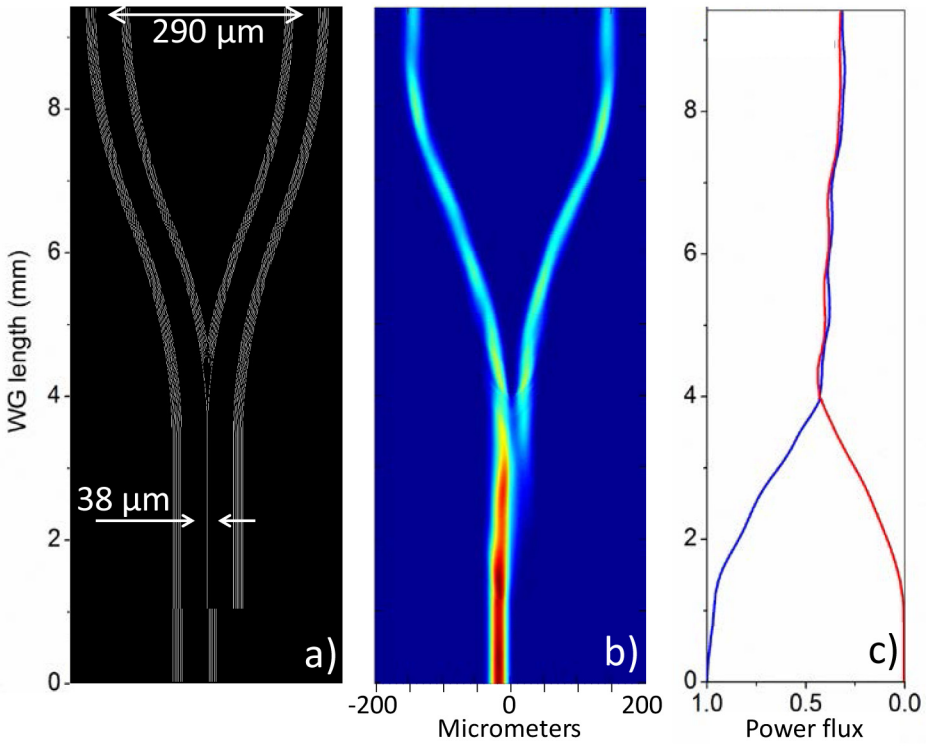

Fig. 9. a) cladding design of the splitter, b) light propagation simulation showing the field intensity distribution, and c) integrated power flux monitor of the two branches along the splitter length, blue and red curves show the left and right branches, respectively.

5. Conclusions

In this work we have used a heuristic approach for finding an effective simulation model of 3D laser fabricated anisotropically stressed depressed cladding waveguides in $LiNbO_3$ crystals for the wavelength of 3.683 µm. We have first developed our model so as to match the modal behavior of a single mode fabricated waveguide, and later used it to investigate for the first time how to decrease the mid-IR losses of cladding waveguides from the around 3 dB/cm currently reported, to the lower losses required for fabricating full on chip instruments using these type of waveguides. We have specifically evaluated how the anisotropic stress fields arising from the laser writing approach produce a difficulty to overcome intrinsic waveguide birefringence, and we have shown how one can address this problem in a realistic way by using a simulation model which includes the stress-optic dynamics into the leaky modes generation and predicts basic functions such as the bend losses and coupling lengths. We believe this study throws new light into the femtosecond laser writing dynamics in crystalline media and it can prove a valuable contribution to the development of mid-IR 3D waveguide devices inside $LiNbO_3$ non-linear crystals.

Acknowledgments

This work was supported by the Spanish MINECO under project MAT2013-47395-C4-4-R, TEC2014-55948-R and FIS2013-44174-P. Catalan Government 2014SGR1358. European Commission (ACP2-GA-2013-314335-JEDI ACE). F. D. acknowledges additional support 2010-ICREA-02 for excellence in research.

#258038 Received 26 Jan 2016; revised 4 Mar 2016; accepted 13 Mar 2016; published 1 Apr 2016